Environmental Science and Pollution Research (2021) 28:4342–4351
https://doi.org/10.1007/s11356-020-10807-y

RESEARCH ARTICLE

# Lanthanum molybdate/magnetite for selective phosphate removal from wastewater: characterization, performance, and sorption mechanisms

Feng Luo[1] · Xiaonan Feng[1] · Xiaoqing Jiang[1,3] · Aijiao Zhou[1] · Pengchao Xie[1] · Zongping Wang[1] · Tao Tao[1] · Jun Wan[2]

Received: 15 June 2020 / Accepted: 9 September 2020 / Published online: 17 September 2020


## Abstract

Lanthanum molybdate/magnetite (M-$La_2(MoO_4)_3$) with various $LaCl_3/Fe_3O_4$ mass ratios was synthesized and optimized for selective phosphate removal from wastewater. M-$La_2(MoO_4)_3$ (2:1) was selected on the basis of phosphate sorption capacity for further experiments and characterized by a variety of methods. The phosphate sorption kinetics, isotherms, and matrix effect were studied. The maximum sorption capacity at initial pH 7 indicates the possible applicability M-$La_2(MoO_4)_3$ (2:1) in removing phosphate from the aquatic environment. Phosphate removal by M-$La_2(MoO_4)_3$ (2:1) with high selectivity was achieved in the presence of other co-existing anions, while calcium and magnesium ions were found to inhibit the sorption process. The sorption isotherm study showed that Freundlich and Sips models fit better the Langmuir model, indicating that heterogeneous multilayer sorption was dominant during the phosphate sorption process. Sorption kinetic results showed that the pseudo-first-order kinetic model can describe well the phosphate sorption process by M-$La_2(MoO_4)_3$ (2:1). Consecutive sorption–desorption runs showed that M-$La_2(MoO_4)_3$ (2:1) could be reused for a few cycles. Simultaneous removal of phosphate and organic matter was achieved in real wastewater by using M-$La_2(MoO_4)_3$ (2:1). The sorption mechanism was inner-sphere complexation.

**Keywords** Phosphate removal · Lanthanum molybdate · Magnetite · Wastewater treatment

## Introduction

Phosphorus (P) is one of the main factors that cause eutrophication in the aquatic environment. Its global reserves are estimated to be exhausted in the next 50–100 years (Cordell et al. 2011; Dox et al. 2019; Peng et al. 2018). Many countries and regions have thus implemented stringent P concentration standards. The USEPA suggested that the total phosphorus (TP) should be below 50 μg P/L in a stream that enters a lake or reservoir (Loganathan et al. 2014); in Australian and New Zealand, it was recommended that the TP concentration should be < 10–25 μg P/L in freshwater lakes and reservoirs (Loganathan et al. 2014). Therefore, it is necessary to develop highly efficient methods to realize phosphate removal to a low level and recovery from wastewater.

Many efforts and treatment technologies have been applied for P removal. However, traditional biological treatment methods are sensitive to variations in temperature and phosphate concentrations, and chemical precipitation causes excess sludge to achieve the removal of low P concentrations (Othman et al. 2018; Zhou et al. 2018). Sorption is a favorable option because it can remove phosphate effectively even at low P concentrations, although the regeneration is required to achieve a sustainable wastewater treatment (Othman et al. 2018). Many sorbents have been developed for P removal, such as biochar-based materials; however, many of them

Responsible Editor: Roberto Cadaval Jr

**Electronic supplementary material** The online version of this article (https://doi.org/10.1007/s11356-020-10807-y) contains supplementary material, which is available to authorized users.

✉ Xiaonan Feng
xnfeng@hust.edu.cn

✉ Jun Wan
wanjun@wtu.edu.cn

[1] School of Environmental Science & Engineering, Huazhong University of Science and Technology, Wuhan 430074, China

[2] School of Environmental Engineering, Wuhan Textile University, Engineering Research Centre for Clean Production of Textile Dyeing and Printing, Ministry of Education, Wuhan 430200, China

[3] Wuhan Planning & Design Co., LTD., Wuhan 430014, China

suffer from low sorption capacity and poor selectivity (Vikrant et al. 2018). Moreover, co-existing anions and cations in wastewater at concentrations higher than phosphate affect the phosphate sorption process because of electrostatic interaction or formation of outer-sphere complexes (Pan et al. 2009). Therefore, it is desirable to develop a sorbent with high affinity toward phosphate to achieve selective phosphate removal from wastewater.

Recently, lanthanum-based materials have shown unique properties in wastewater treatment, especially, strong affinity toward phosphate sorption (Ghiasi and Malekzadeh 2015; Liu et al. 2018; Wang et al. 2015). La-modified bentonite (Phoslock®) has been used with real water and lakes. Its maximum sorption capacity was only 9.54–10.54 mg/g. Lanthanum/activated carbon (Zhang et al. 2012), lanthanum/graphene (Chen et al. 2016), and lanthanum/hydrogel (Dong et al. 2017) have also been developed to enhance phosphate removal from wastewater. Furthermore, various molybdate-based materials with incorporated lanthanide (e.g., lanthanum molybdate) may have the potential to be used as highly effective sorbents (Bharat et al. 2014); however, there is limited knowledge about the application of $La_2(MoO_4)_3$ for phosphate sorption and real-wastewater treatment.

Magnetic separation could achieve fast separation of magnetic particles from water compared with sedimentation or filtration, and the introduction of $Fe_3O_4$ nanoparticles benefit the separation and recovery of adsorbents. Although some $Fe_3O_4$-based adsorbents have been developed for phosphate removal, low sorption capacity and poor selectivity toward phosphate restrict their performance in real wastewater (Fang et al. 2017).

Therefore, the objectives of this study are to (1) synthesize and optimize magnetic $La_2(MoO_4)_3/Fe_3O_4$ nanocomposites through a hydrothermal method for phosphate removal, (2) to examine the selectivity of $La_2(MoO_4)_3/Fe_3O_4$ in phosphate removal, and (3) to elucidate phosphate sorption mechanisms by incorporating batch experiments and spectroscopic investigations. This study provides a new sorbent for selective phosphate sorption from wastewater.

## Materials and methods

### Chemicals

Iron(III) chloride hexahydrate ($FeCl_3{\cdot}6H_2O$, ≥ 99%), trisodium citrate (98%), ethylene glycol (≥ 99.5%), sodium acetate (≥ 99%), lanthanum(III) chloride hydrate ($LaCl_3{\cdot}xH_2O$, ≥ 99%), ammonium molybdate tetrahydrate ($(NH_4)_6Mo_7O_{24}{\cdot}4H_2O$, ≥ 99%), and potassium dihydrogen phosphate ($KH_2PO_4$, ≥ 99.5%) were obtained from Sinopharm Chemical Reagent Co. (Shanghai, China). All other chemicals were analytical reagents (AR) and used as received. Deionized (DI) water produced by an ultrapure water system (Pcdxj-10, Pincheng, China) was used in all experiments.

### Synthesis of $Fe_3O_4$ nanoparticles and $La_2(MoO_4)_3/Fe_3O_4$ nanocomposites

$Fe_3O_4$ particles were synthesized as follows (Chen et al. 2010): 50 mL of ethylene glycol was mixed with 1.5 g of $FeCl_3{\cdot}6H_2O$, 0.36 g of trisodium citrate, and 2.4 g of sodium acetate, followed by stirring for 1 h at room temperature. The mixture was then transferred into a Teflon-lined stainless-steel autoclave (100 mL capacity) for heating at 200 °C for 10 h. After cooling down to room temperature, the black products ($Fe_3O_4$) were washed with ethanol and with deionized water three times, and then dried under vacuum.

$La_2(MoO_4)_3/Fe_3O_4$ nanocomposites were prepared according to Li et al. (2017) and Wu et al. (2017) with a few modifications. $LaCl_3{\cdot}xH_2O$ (0.45 g) and 0.04 mol/L $(NH_4)_6Mo_7O_{24}$ (10 mL) were separately added into the $Fe_3O_4$ suspension (0.45 g of $Fe_3O_4$ nanoparticles in 10 mL of DI water). The above mixture was first stirred for 5 h at 25 °C and then transferred to a 100 mL of Teflon-lined stainless-steel autoclave. After reaction at 180 °C for 12 h and then cooling to room temperature, the final products were washed with deionized water three times and dried under vacuum. $La_2(MoO_4)_3/Fe_3O_4$ nanocomposites with different $LaCl_3/Fe_3O_4$ mass ratios (1:1, 2:1 and 5:1) were also prepared with the same method.

### Characterization of magnetic sorbents

Scanning electron microscopy (SEM) images of the composites were recorded on a Zeiss Sigma 300 electron microscope (German) operated at 10-kV accelerating voltage. The transmission electron microscopy (TEM) images were collected by using a JEOL 2010 microscope (Japan) with an accelerating voltage of 200 kV. The crystal structures of composites were detected by X-ray powder diffraction (XRD; Shimadzu XRD-7000, Japan). The magnetic properties were measured with a vibrating sample magnetometer (VSM, MPMS Squid, Quantum Design, USA). The porous properties were measured by nitrogen adsorption-desorption isotherms analysis (based on the BET isotherm calculation) with a Micromeritics ASAP 2460 (USA). The functional groups on the surface of the composites were examined by Fourier transform infrared spectroscopy (FT-IR; Bruker Vertex 70, Germany) with KBr pellets. X-ray photoelectron spectroscopy (XPS; Escalab 250xi, Thermo, USA) was used to detect the binding energy of composites before and after phosphate sorption, and the binding energy was calibrated with the C 1 s peak at 284.8 eV.

## Batch experiments

Batch experiments were conducted to explore the phosphate sorption performance of M-$La_2(MoO_4)_3$. The sorption kinetics study was carried out by mixing 0.25 g of sorbents and 500 mL of phosphate solution (5 mg P/L, pH = 7) with mechanical stirring at 300 rpm. The appropriate amount of the supernatant was sampled at various time intervals for P concentration measurement after it was filtered through a 0.22-μm membrane. For sorption isotherm study, a dosage of 0.1 g/L sorbents was used to investigate the phosphate sorption capacity in 100-mL serum bottles with initial phosphate concentrations ranging from 3 to 20 mg P/L (pH = 7). These vials were shaken in a water bath shaker (25 °C) for 24 h at 140 rpm.

The pH effect studies were carried out by adjusting the initial pH of phosphate solution (5 mg P/L) from 3 to 11 ± 0.1 using 0.1 M HCl or 0.1 M NaOH solution. The leached La, Mo, and Fe ions concentrations from the composites after phosphate sorption equilibrium were also tested (see "Analytical methods" section). The phosphate sorption selectivity was conducted by comparing the sorption capacity of M-$La_2(MoO_4)_3$ in the presence of co-existing $Cl^-$, $NO^{3-}$, $SO_4^{2-}$, $HCO_3^-$, $Ca^{2+}$, and $Mg^{2+}$. These ions were present within their typical concentrations in wastewater, i.e., $Ca^{2+}$ and $Mg^{2+}$ were at 4–70 mg/L, while the anions ranged from 5 to 100 mg/L (Othman et al. 2018). The vials containing the initial concentration of 5 mg P/L phosphate solution (pH = 7) and 0.1 g/L sorbents were shaken in the shaker at 140 rpm and 25 °C for 24 h. The phosphate-loaded sorbents were separated from water and collected by using a magnet and then dispersed in 20 mL of 1 M NaOH solution for 24 h at 25 °C. The regenerated M-$La_2(MoO_4)_3$ was washed with DI water until neutral pH and reused in the succeeding sorption–desorption cycles. A ratio of the amount of desorbed to the initially sorbed phosphate was applied as the phosphate desorption efficiency.

## Modeling and data analysis

The phosphate sorption capacity removal efficiency of M-$La_2(MoO_4)_3$ was calculated with Eqs. (1) and (2), respectively (Wan et al. 2017).

$$q_t = \frac{(C_0 - C_t) \times V}{m} \tag{1}$$

$$R(\%) = \frac{C_0 - C_t}{C_0} \times 100\% \tag{2}$$

where $q_t$ is the sorption capacity (mg P/g) of M-$La_2(MoO_4)_3$ at time $t$ (min), $R(\%)$ is the phosphate removal efficiency, $C_0$ is the initial phosphate concentration (mg P/L), $C_t$ is phosphate concentration (mg P/L) at time $t$ (min), $V$ is the volume of the prepared phosphate solution (L); and $m$ is the mass of sorbent (g).

The kinetic results were fitted with pseudo-first-order (Eq. (3)) and pseudo-second-order (Eq. (4)) kinetic models (Tran et al. 2017).

$$q_t = q_e\left(1 - e^{-k_1 t}\right) \tag{3}$$

$$q_t = \frac{k_2 {q_e}^2 t}{1 + k_2 q_e t} \tag{4}$$

where $q_e$ and $q_t$ are the phosphate sorption capacity at equilibrium and at time $t$ (min), respectively; $k_1$ ($min^{-1}$) is the rate constant of the pseudo-first-order model, and $k_2$ (g/mg-min) is the rate constant of the pseudo-second-order model.

The sorption isotherm data was fitted with Langmuir (Eq. (5)), Freundlich (Eq. (6)), Sips (Eq. (7)), and Dubinin–Radushkevich (D-R) (Eq. (8)) models (Rostamian et al. 2011; Tran et al. 2017).

$$q_e = \frac{q_m K_L C_e}{1 + K_L C_e} \tag{5}$$

$$q_e = K_f {C_e}^{n_f} \tag{6}$$

$$q_e = \frac{Q_s K_s C_e^{1/n}}{1 + K_s C_e^{1/n}} \tag{7}$$

$$q_e = q_{DR} \exp\left\{-K_{DR}\left[RT \ln\left(1 + \frac{1}{C_e}\right)\right]^2\right\} \tag{8}$$

herein, $q_e$ is the equilibrium sorption capacity of phosphate (mg P/g), $C_e$ is the equilibrium phosphate concentration (mg P/L); $q_m$ is the maximum phosphate sorption capacity calculated from the Langmuir model (mg P/g); $K_L$ is the Langmuir constant (L/mg P); $K_f$ is the Freundlich constant ((mg P/g)(L/mg P)$^{1/nf}$), and $n_f$ is the heterogeneity factor. $Q_s$, $K_s$, and $1/n$ are maximum sorption capacity (mg P/g), equilibrium constant (L/mg), and exponent of the Sips model, respectively. $q_{DR}$ and $K_{DR}$ are the sorption capacity (mg P/g) and constant ($mol^2/kJ^2$), respectively, related to the sorption energy of the D-R model. $R$ is the gas constant (8.314 J/mol-K) and $T$ is the temperature (K).

## Analytical methods

The phosphate concentration was measured with the ammonium molybdate method by using a UV/vis spectrometer (UV-1600PC, Mapada, China) at a wavelength of 700 nm. The concentrations of typical anions in this study were

determined using ion chromatography (ICS-1100, Thermo Scientific, USA). Total organic carbon (TOC) of Huxi River in Wuhan, China, was analyzed using a TOC analyzer (Muclti N/C 2100, Jena, Germany). The concentrations of cations (in water and wastewater) and leached La, Mo, and Fe ions were measured using an inductively coupled plasma optical emission spectrometer (ICP-OES; Optima 8300 DV, Perkin-Elmer, USA).

## Results and discussion

### Optimizing the La/Fe mass ratio of M-$La_2(MoO_4)_3$ for phosphate sorption

Figure 1 shows the phosphate sorption capacity differences of $La_2(MoO_4)_3/Fe_3O_4$ nanocomposite with different mass ratios. Pure $Fe_3O_4$ was also tested for comparison. Using $LaCl_3$ alone formed bare $La_2(MoO_4)_3$, which had a highest phosphate sorption capacity compared with $Fe_3O_4$ and $La_2(MoO_4)_3/Fe_3O_4$ nanocomposites. Phosphate sorption capacity of M-$La_2(MoO_4)_3$ increased from 25.33 to 31.57 mg-P/g as the $LaCl_3/Fe_3O_4$ mass ratio varied from 1:1 to 5:1, and phosphate sorption capacities of the M-$La_2(MoO_4)_3$ were up to eight times that of pure $Fe_3O_4$. These results imply that $La_2(MoO_4)_3$ was the dominant component of M-$La_2(MoO_4)_3$ for phosphate sorption, and that the contribution of $Fe_3O_4$ to phosphate removal appeared to be minor. To minimize La usage, $La_2(MoO_4)_3/Fe_3O_4$ (2:1) was selected for further sorption tests and characterization.

### Characterization of $La_2(MoO_4)_3/Fe_3O_4$ nanocomposite

Transmission electron microscopy image of $Fe_3O_4$ and electron microscopy of M-$La_2(MoO_4)_3$ (2:1) are depicted in Fig. 2.

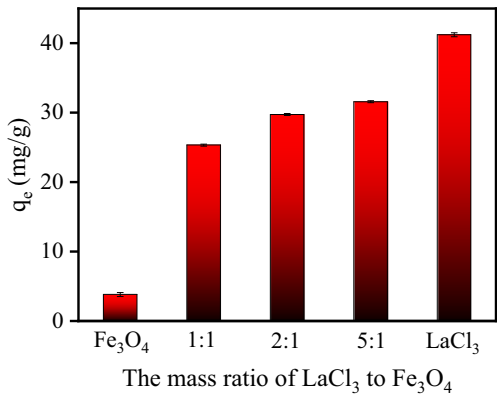


**Fig. 1** Phosphate sorption capacity of the $La_2(MoO_4)_3/Fe_3O_4$ nanocomposites with different $LaCl_3/Fe_3O_4$ mass ratios. Experimental conditions for sorption experiments: dosage of sorbent: 0.1 g/L; initial phosphate concentration: 5 mg P/L; pH: 7.0; temperature: 25 °C

The particle size of $Fe_3O_4$ was ~ 200 nm (Fig. 2a), and the $Fe_3O_4$ nanoparticles exhibited a well monodisperse feature. After loading of $La_2(MoO_4)_3$, the $Fe_3O_4$ nanoparticles were successfully entrapped within the $La_2(MoO_4)_3$ nanoparticles. The particle size of $La_2(MoO_4)_3$ was ~ 700 nm, which was much smaller than that of the previous study (Bu et al. 2007).

The XRD patterns of $La_2(MoO_4)_3/Fe_3O_4$ before and after P sorption are shown in Fig. 3. The characteristic peaks at 27.9°, 33.5°, and 45.7° can be indexed to the (112), (200), and (204) planes of the body-centered tetragonal $La_2(MoO_4)_3$ phase (JCPDS No.045-0407) (Ding et al. 2010). The characteristic peaks at 35.5°, 43.1°, and 63.0° can be indexed to the (311), (400), and (440) planes of the cubic $Fe_3O_4$ phase (JCPDS no. 019-0629) (Fang et al. 2017); this demonstrates that the $La_2(MoO_4)_3/Fe_3O_4$ nanocomposites have the crystal structure of both $La_2(MoO_4)_3$ and $Fe_3O_4$.

The BET analysis of $Fe_3O_4$ and M-$La_2(MoO_4)_3/Fe_3O_4$ (2:1) is listed in Table S1. The results show that the incorporation of $La_2(MoO_4)_3$ caused a decline of the surface area for $Fe_3O_4$ particles from 61.98 to 20.81 $m^2/g$, which probably resulted from nanocomposite aggregation and increased the particle size (Wu et al. 2017). The total pore volume of $Fe_3O_4$ and $La_2(MoO_4)_3/Fe_3O_4$ (2:1) were 0.14 and 0.05 $cm^3/g$, respectively.

The VSM analysis indicated the superparamagnetic property of M-$La_2(MoO_4)_3$ (2:1) nanocomposites (Fig. 4a), which can benefit sorbent separation and redispersion for phosphate sorption and recovery (Fang et al. 2018). The saturation magnetization value of M-$La_2(MoO_4)_3$ (2:1) was 19.07 emu/g, which was less than that of 75.00 emu/g for $Fe_3O_4$, but was sufficient to separate the M-$La_2(MoO_4)_3$ (2:1) from water (Fig. 4b). Similar results were also shown in other studies (Fang et al. 2018; Hao et al. 2019).

### Phosphate sorption by $La_2(MoO_4)_3/Fe_3O_4$ (2:1) nanocomposite

#### Sorption kinetics

Figure 5a and Table S2 show the kinetic results of phosphate sorption by the M-$La_2(MoO_4)_3$ (2:1). There is fast phosphate uptake in the initial 6 h, with the removal efficiency reaching 66%, and then the sorption process gradually reached equilibrium within 24 h. Table S2 shows that the correlation coefficient ($R^2$) for the pseudo-first-order and pseudo-first-order kinetic models were 0.987 and 0.982, respectively, implying that both kinetic models could fit well the experimental kinetic data. However, the predicted equilibrium sorption capacity of the pseudo-first-order kinetic model (8.37 mg P/g) was closer to the experimental data (8.63 mg P/g) as compared with the pseudo-second-order kinetic model (9.91 mg P/g). Thus, the pseudo-first-order model better described the kinetic sorption experimental results.

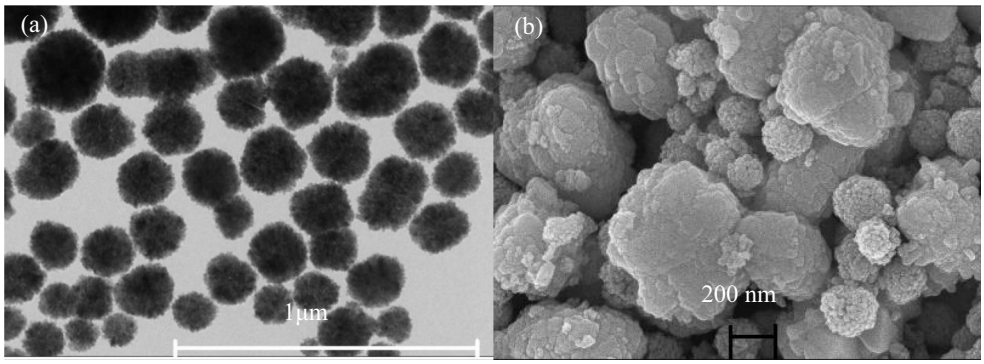


**Fig. 2** TEM image of $Fe_3O_4$ nanoparticles (**a**) and SEM image of $La_2(MoO_4)_3/Fe_3O_4$ (2:1) nanocomposites (**b**)

## Sorption isotherms

Langmuir, Freundlich, Sips, and D-R models were used to fit the phosphate sorption experimental data, as shown in Fig. 5b and Table S3. According to the $R^2$ differences between the four models, the experimental result matched the sorption isotherms in the following sequence: Sips > Freundlich > Langmuir > D-R isotherm model. The value of $1/n = 0.56$ (< 1) indicated that the isotherm was more of a Freundlich form rather than Langmuir (Dong and Wang 2016). Therefore, P sorption by M-$La_2(MoO_4)_3$ (2:1) might be heterogeneous multilayer sorption. The maximum phosphate sorption capacity calculated by the Sips model was 84.39 mg P/g. Compared with other sorbents, the maximum phosphate sorption capacity of M-$La_2(MoO_4)_3$ (2:1) was relatively high, as shown in Table S4.

## Effects of coexisting ions

High selectivity is a favorable property of sorbents for phosphate removal and recovery. However, the co-existing ions in sewage may compete for the sorption sites on the surface of sorbents and interfere in the sorption process. Figure 5 c shows the sorption performances for phosphate by the M-$La_2(MoO_4)_3$ (2:1) in the presence of these ions. It was obvious that $Cl^-$, $NO_3^-$, and $SO_4^{2-}$ exhibited negligible effects on the phosphate sorption capacity of M-$La_2(MoO_4)_3$ (2:1), and that $HCO_3^-$ could enhance the phosphate sorption capacity. The molar ratio of competing anions to phosphate such as $Cl^-$, $NO_3^-$, and $SO_4^{2-}$ was up to 15, indicating the highly selective sorption for phosphate by M-$La_2(MoO_4)_3$ (2:1). The results were similar to phosphate sorption by other La-based materials due to the affinity of La towards phosphate (Hao et al. 2019; Su et al. 2015), which was reasonably interpreted via the inner-sphere complexation mechanisms (see "Reusability of La2(MoO4)3/Fe3O4(2:1) nanocomposite and phosphate

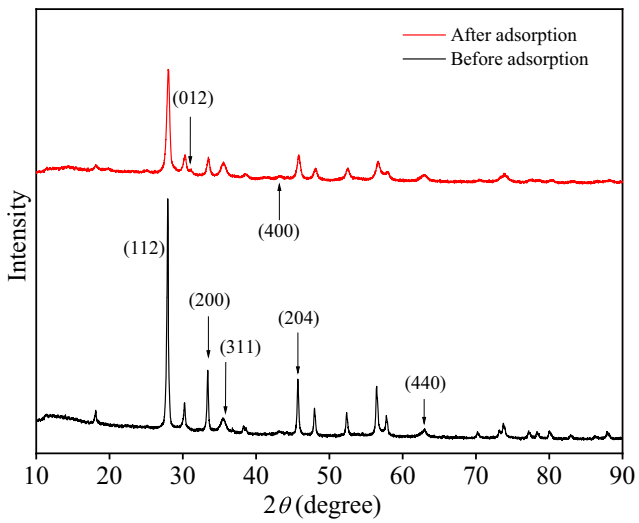


**Fig. 3** XRD diffraction patterns of $La_2(MoO_4)_3/Fe_3O_4$ (2:1) before and after P sorption

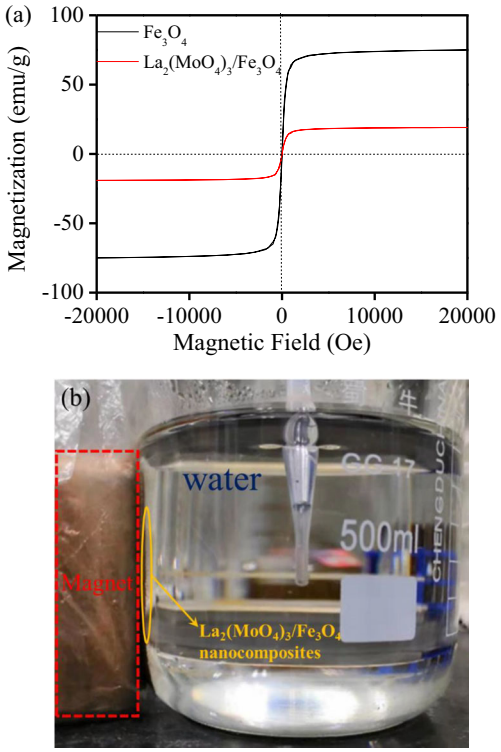


**Fig. 4** VSM analysis of $Fe_3O_4$ nanoparticles and $La_2(MoO_4)_3/Fe_3O_4$ (2:1) nanocomposite (**a**), and digital photograph of $La_2(MoO_4)_3/Fe_3O_4$ (2:1) nanocomposite in response to a permanent magnet after 5 min (**b**)

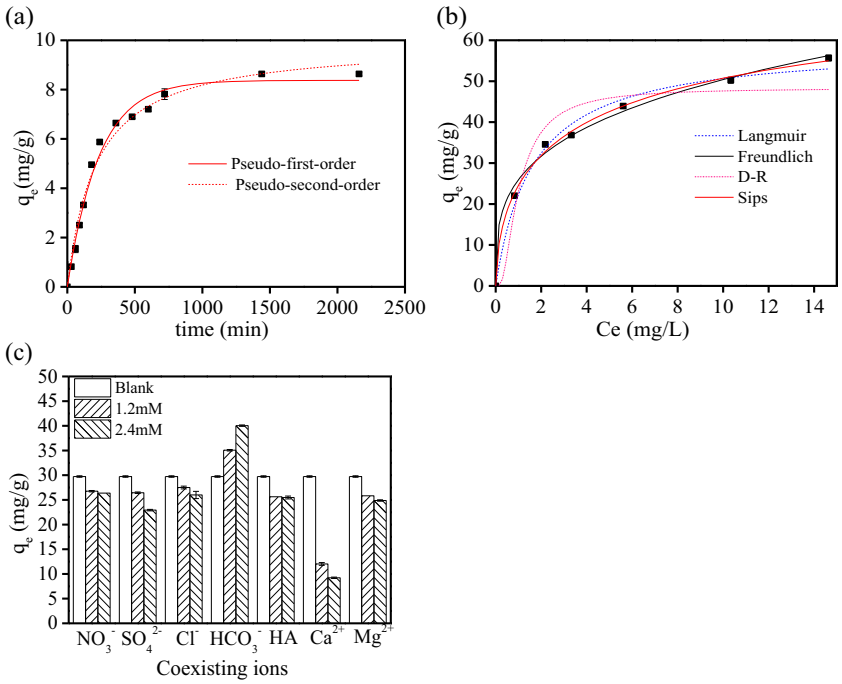


**Fig. 5** Phosphate sorption kinetics (**a**), isotherms (**b**), and effects of coexisting ions on phosphate sorption by M-$La_2(MoO_4)_3/Fe_3O_4$ (2:1) (**c**). Experimental conditions: **a** 0.5 g/L, 5 mg P/L, pH 7.0, 25 °C; **b** 0.1 g/L, 3–20 mg P/L, pH 7.0, 25 °C; **c** 0.1 g/L, 5 mg P/L, pH 7.0, 25 °C

removal from real water" section). Compared with the outer-sphere complexation, the increasing ionic strength can hardly affect inner-sphere complexation, which can overcome the competitive sorption from background ions (Ding et al. 2010; Fang et al. 2018). However, $Ca^{2+}$ and $Mg^{2+}$ showed a negative effect on phosphate sorption by M-$La_2(MoO_4)_3$ (2:1), and the calcium-induced effect was stronger. The surface of M-$La_2(MoO_4)_3$ (2:1) was negatively charged at pH 7.0 (see "Effects of solution pH" section), and we removed phosphate via ligand exchange of the hydroxyl groups on the sorbents surface. $Ca^{2+}$ and $Mg^{2+}$ may also compete for the hydroxyl groups. Therefore, the available number of hydroxyl groups on the surface of sorbents is less, possibly suppressing the phosphate sorption process (Lin et al. 2019; Suresh Kumar et al. 2018).

### Effects of solution pH

The pH effect on phosphate sorption by the M-$La_2(MoO_4)_3$ (2:1) was investigated and presented in Fig. 6. When the initial pH ranged from 3 to 10, the phosphate uptake first increased and then decreased. The maximum reached pH 7.0 with a sorption capacity of 29.73 mg-P/g (Fig. 6b). Zhang et al. (Zhang et al. 2011) also found that the amount of phosphate increased at pH 2.0–3.0 and maintained this level between pH 3.0 and 7.0, followed by a deceased sorption capacity between pH 10.0 and 2.0. Other La-based sorbents also presented similar performances in phosphate sorption (He et al. 2015). Figure 6a shows that a $pH_{pzc}$ of M-$La_2(MoO_4)_3$ (2:1) was around 4.0, indicating that the surface of the sorbent was positively charged when the pH was below 4.0, and negatively charged when pH was below 4.0. At pH 3.0, $H_2PO_4^-$ is the major species with a small amount of $H_3PO_4$, which can barely be adsorbed by M-$La_2(MoO_4)_3$ (2:1). Furthermore, the high lanthanum leaching concentration of M-$La_2(MoO_4)_3$ (2:1) also led to relative low sorption capacities. As the pH increased from 3.0 to 4.0, the proportion of $H_3PO_4$ decreased and that of $H_2PO_4^-$ rapidly peaked. The positively charged surface is beneficial to phosphate removal by electrostatic attraction, thus enhancing the phosphate sorption capacity. When the pH was above 4.0, the surface of M-$La_2(MoO_4)_3$ (2:1) was negatively charged; thus, the phosphate removal was mainly attributed to ligand exchange (discussed in "Reusability of La2(MoO4)3/Fe3O4(2:1) nanocomposite and phosphate removal from real water" section). In the pH range of 7.0–11.0, the phosphate sorption capacity also decreased because the dominantly divalent $HPO_4^{2-}$ has a lower affinity to the sorbents (Shi et al. 2019).

## Reusability of $La_2(MoO_4)_3/Fe_3O_4$ (2:1) nanocomposite and phosphate removal from real water

The exhausted M-$La_2(MoO_4)_3$ (2:1) from phosphate was regenerated by various solutions, as shown in Fig. S2(a). P desorption was very low in alkaline conditions; this could be attributed to the formation of $LaPO_4$ via ligand exchange (see "Removal mechanisms of phosphate by M-La2(MoO4)3 (2:1)" section). Though coexistence of $OH^-$ (pH 11.0) hindered the sorption of phosphate (Fig. 6b); the complex could not be desorbed by $OH^-$ (1 M NaOH), once the phosphate was adsorbed by sorbents. The desorption efficiency increased from 11.98% in 0.01 M HCl to 88.88%. The reusability of

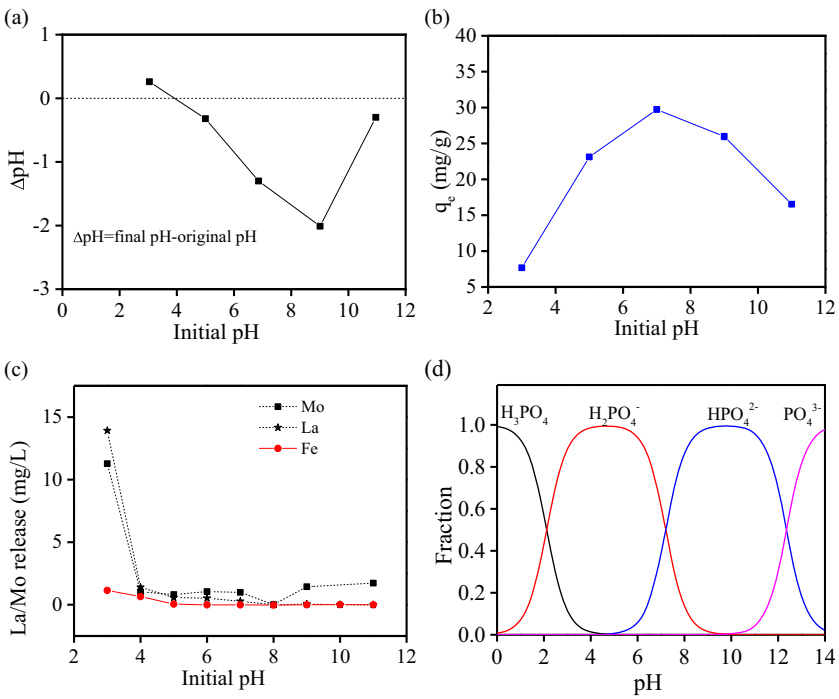


**Fig. 6** **a** Plot of ΔpH (= final pH − initial pH) versus initial pH. **b**Effects of pH on phosphate sorption by the M-$La_2(MoO_4)_3$/$Fe_3O_4$ (2:1). **c** La, Mo, and Fe ions leaching at different initial pH levels. **d** Distribution of phosphate species as a function of pH. Experimental conditions: 0.1 g/L, 5 mg P/L, 25 °C

the M-$La_2(MoO_4)_3$ (2:1) was enhanced under acid conditions because of the release of $LaPO_4$.

Eight successive sorption–desorption cycles were conducted to evaluate the reusability of the M-$La_2(MoO_4)_3$ (2:1) in phosphate removal. The desorption efficiency ranged between 14.81 and 106.91% during the eight cycles, and we observed a 30% decrease in the sorption capacity in the eighth cycle. The enhancement of sorption capacity during the second cycle was possibly due to the conversion from $La_2(MoO_4)_3$ to $La(OH)_3$ phase under conditions with excess $OH^-$, which can be proved by the XRD pattern after the desorption process (Fig. S3). Thus, more efforts are necessary for developing the effective regenerating solution with more than 1 M NaOH solution to increase the phosphate desorption efficiency such as high-temperature and high-pressure conditions (Xie et al. 2014).

M-$La_2(MoO_4)_3$/$Fe_3O_4$ (2:1) was also applied for real water and phosphate, and natural organic matter sorption was tested. The characteristics of the Huxi River in Wuhan, China are shown in Table S5. As shown in Fig. S4, the phosphate removal rate increased from 20.67 to 56.72% when the M-$La_2(MoO_4)_3$/$Fe_3O_4$ (2:1) dosage increased from 0.1 to 0.5 g/L. Considering that the organic matter existed widely in the aquatic environment (Hao et al. 2019), we also performed simultaneous removal of phosphate and organic matter. The results showed that the TOC removal efficiency was around a stable level of 56.74%. No uptake of anions such as $Cl^-$, $SO_4^{2-}$, and $NO_3^-$ was detected by ion chromatography method, which was in accordance with the highly selective sorption of phosphate as mentioned above. These results demonstrate the potential of using M-$La_2(MoO_4)_3$ (2:1) as a recoverable sorbent for selective phosphate removal to a low level for real-wastewater treatment.

## Removal mechanisms of phosphate by M-$La_2(MoO_4)_3$ (2:1)

A series of complementary analysis was performed to explore the sorption mechanisms of phosphate by M-$La_2(MoO_4)_3$ (2:1). Figure 7 shows the FTIR results of the M-$La_2(MoO_4)_3$ (2:1) before and after phosphate sorption (neutral pH) in terms of functional groups. The broadband at around 3432 $cm^{-1}$ represents the O–H vibration (Ding et al. 2010). The peak at 711 $cm^{-1}$ is in accordance with the Mo–O bond (Li et al.

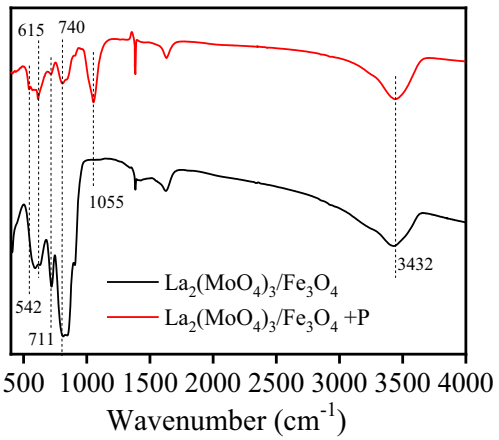


**Fig. 7** Fourier transform infrared spectra of $La_2(MoO_4)_3$/$Fe_3O_4$ (2:1) before and after 5 mg P/L phosphate adsorption

2017), and the band below 740 $cm^{-1}$ is attributable to the Mo–O–Mo vibration (Bharat et al. 2014). A new peak at about 1055 $cm^{-1}$ appearing after phosphate sorption is due to the P–O vibration from the $PO_4^{3-}$ group (Shi et al. 2019). Also, the new peaks at 615 and 542 $cm^{-1}$ resulted from the O–P–O vibration (Zhang et al. 2012), which implies the formation of inner-sphere complexation between phosphate and sorbents via ligand exchange.

The surface complexation of phosphate with M-$La_2(MoO_4)_3$ (2:1) was further investigated by XPS analysis. Figure 8 presented the wide-scan and high-resolution XPS spectra of M-$La_2(MoO_4)_3$ (2:1) nanocomposites before and after phosphate sorption. Both the wide-scan and P 2p high-resolution XPS spectra showed a new peak that appeared at 133.9 eV after phosphate sorption, suggesting the chemical bonding of phosphate and M-$La_2(MoO_4)_3$ (2:1) (Fig. 8a–c). Figure 8d shows that the typical peaks of both La 3d5/2 and La 3d3/2 shifted by 0.6–0.7 eV to higher values after phosphate sorption, implying the formation of La–O–P inner-sphere complexation, which caused the electron transfer in the valence band of La 3d (Shi et al. 2019; Wu et al. 2017). It was noted that the satellite energy separation of La 3d5/2 after phosphate sorption (3.6 eV) was similar to that of $LaPO_4{\cdot}xH_2O$ (Sunding et al. 2011). Figure 3 also shows that the presence of a new peak at 31.0° after phosphate sorption is in accordance with the (012) planes of the $LaPO_4$ phase (JCPDS No.032-0493). These results confirmed that $LaPO_4$ formed during phosphate sorption by M-$La_2(MoO_4)_3$ (2:1).

Figure 8e and f show the O 1 s high-resolution XPS spectra before and after phosphate sorption, and Table S6 lists the fitted peak parameters. The O 1 s XPS fitting peaks at 530.4, 531.4, and 533.3 eV correspond to $O^{2-}$, $OH^-$/O–P, and $H_2O$, respectively (Fang et al. 2015; Shi et al. 2019). The $OH^-$/O–P content increases from 26.80 to 63.22%, and the $O^{2-}$ decreases from 65.94 to 36.78% after phosphate sorption was possibly due to the binding of phosphate with La–O or Fe–O, and the La–O–P and Fe–O–P inner-sphere complexation occurred (Fang et al. 2018).

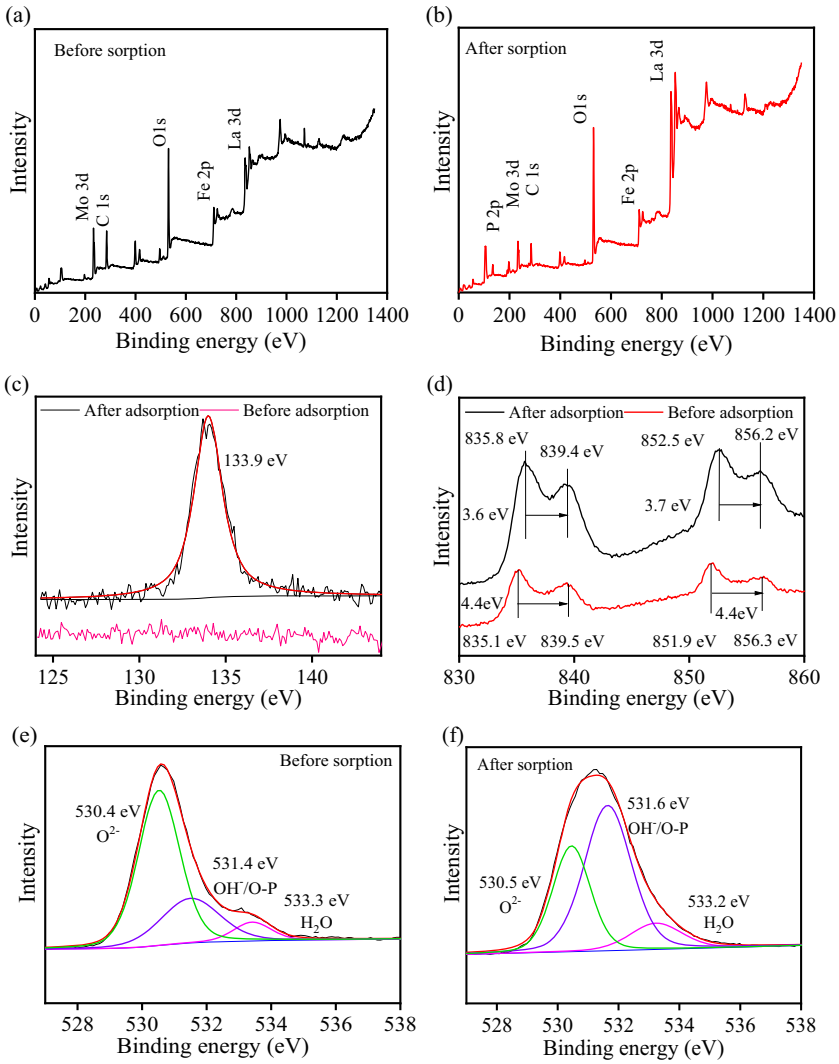


**Fig. 8** X-ray photoelectron spectroscopic spectra of $La_2(MoO_4)_3/Fe_3O_4$ (2:1) before and after 5 mg/L phosphate adsorption: **a**, **b** wide scan, **c** P 2p region, **d** La 3d region, and **e**, **f** O 1 s region

## Implications

Magnetic M-$La_2(MoO_4)_3$ nanocomposites can be used for effective phosphate removal from wastewater in batch tests. Considering the real conditions phosphate removal from wastewater or natural water in a continuous mode, a fluidized bed process combined with a magnetic separation unit will achieve the sustainable phosphate removal and recovery. To achieve this goal, it is necessary to conduct a pilot-scale experiment, and investigate (1) the production of this type of sorbent in commercial scale, (2) the environment and economic aspects of the sorbent (3) phosphate recovery and sorbent reuse. and (4) the comparison of its performance and cost-effectiveness with other sorbents.

## Conclusion

Magnetic M-$La_2(MoO_4)_3$ nanocomposites were fabricated and optimized for selective phosphate removal from wastewater. M-$La_2(MoO_4)_3$ (2:1) exhibited a high sorption capacity, favorable magnetic separation property and good selectivity for phosphate in the presence of competing ions. The pseudo-first-order kinetic model could better describe the phosphate sorption process by M-$La_2(MoO_4)_3$ (2:1), and we achieved the sorption equilibrium at 24 h. The sorption tests show that the maximum sorption capacity reached at pH 7.0. Overall, these findings implied that M-$La_2(MoO_4)_3$ (2:1) exhibited potential for application in wastewater treatment. The FTIR, XRD, and XPS spectra showed that phosphate sorption was attributed to the formation of inner-sphere complexation.

**Acknowledgments** The authors thank the Analytical and Testing Center of the Huazhong University of Science and Technology for related analyses.

**Funding** This study is funded by the National Natural Science Foundation of China (grant no. 51608216), Natural Science Foundation of Hubei Province, China (grant no. 2020CFB383) and the Fundamental Research Funds for the Central Universities, HUST (grant no. 2016YXMS289).

## References

Bharat LK, Rao BV, Yu JS (2014) Polyol mediated solvothermal synthesis and characterization of spindle shaped $La_2(MoO_4)_3$: $Eu^{3+}$ phosphors. Chem Eng J 255:205–213

Bu W, Xu Y, Zhang N, Chen H, Hua Z, Shi J (2007) Controlled construction of uniform pompon-shaped microarchitectures self-assembled from single-crystalline lanthanum molybdate nanoflakes. Langmuir 23:9002–9007

Chen H, Deng C, Zhang X (2010) Synthesis of $Fe_3O_4$@$SiO_2$@PMMA core–shell–shell magnetic microspheres for highly efficient enrichment of peptides and proteins for MALDI-ToF MS analysis. Angew Chem Int Ed 49:607–611

Chen M, Huo C, Li Y, Wang J (2016) Selective adsorption and efficient removal of phosphate from aqueous medium with graphene–lanthanum composite. ACS Sustain Chem Eng 4:1296–1302

Cordell D, Rosemarin A, Schröder JJ, Smit AL (2011) Towards global phosphorus security: A systems framework for phosphorus recovery and reuse options. Chemosphere 84:747–758

Ding Y, Li C, Guo R (2010) Facile fabrication of pomponlike microarchitectures of lanthanum molybdate via an ultrasound route. Ultrason Sonochem 17:46–54

Dong S, Wang Y (2016) Characterization and adsorption properties of a lanthanum-loaded magnetic cationic hydrogel composite for fluoride removal. Water Res 88:852–860

Dong S, Wang Y, Zhao Y, Zhou X, Zheng H (2017) $La^{3+}$/$La(OH)_3$ loaded magnetic cationic hydrogel composites for phosphate removal: Effect of lanthanum species and mechanistic study. Water Res 126:433–441

Dox K, Everaert M, Merckx R, Smolders E (2019) Optimization of phosphate recovery from urine by layered double hydroxides. Sci Total Environ 682:437–446

Fang L, Huang L, Holm PE, Yang X, Hansen HCB, Wang D (2015) Facile upscaled synthesis of layered iron oxide nanosheets and their application in phosphate removal. J Mater Chem A 3:7505–7512

Fang L, Wu B, Lo IMC (2017) Fabrication of silica-free superparamagnetic $ZrO_2$@$Fe_3O_4$ with enhanced phosphate recovery from sewage: performance and adsorption mechanism. Chem Eng J 319:258–267

Fang L, Liu R, Li J, Xu C, Huang L, Wang D (2018) Magnetite/Lanthanum hydroxide for phosphate sequestration and recovery from lake and the attenuation effects of sediment particles. Water Res 130:243–254

Ghiasi M, Malekzadeh A (2015) Synthesis, characterization and photocatalytic properties of lanthanum oxy-carbonate, lanthanum oxide and lanthanum hydroxide nanoparticles. Superlattice Microst 77:295–304

Hao H, Wang Y, Shi B (2019) $NaLa(CO_3)_2$ hybridized with $Fe_3O_4$ for efficient phosphate removal: Synthesis and adsorption mechanistic study. Water Res 155:1–11

He J, Wang W, Sun F, Shi W, Qi D, Wang K, Shi R, Cui F, Wang C, Chen X (2015) Highly efficient phosphate scavenger based on well-dispersed $La(OH)_3$ nanorods in polyacrylonitrile nanofibers for nutrient-starvation antibacteria. ACS Nano 9:9292–9302

Li F, Liu S, Qi R, Li H, Cui T (2017) Effective visualization of latent fingerprints with red fluorescent $La_2(MoO_4)_3$: $Eu^{3+}$ microcrystals. J Alloys Compd 727:919–924

Lin J, Wang X, Zhan Y (2019) Effect of precipitation pH and coexisting magnesium ion on phosphate adsorption onto hydrous zirconium oxide. J Environ Sci 76:167–187

Liu X, Zong E, Hu W, Song P, Wang J, Liu Q, Ma Z, Fu S (2018) Lignin-derived porous carbon loaded with $La(OH)_3$ nanorods for highly efficient removal of phosphate. ACS Sustain Chem Eng 7:758–768

Loganathan P, Vigneswaran S, Kandasamy J, Bolan NS (2014) Removal and recovery of phosphate from water using sorption. Crit Rev Environ Sci Technol 44:847–907

Othman A, Dumitrescu E, Andreescu D, Andreescu S (2018) Nanoporous Sorbents for the Removal and Recovery of Phosphorus from Eutrophic Waters: Sustainability Challenges and Solutions. ACS Sustain Chem Eng 6:12542–12561

Pan B, Wu J, Pan B, Lv L, Zhang W, Xiao L, Wang X, Tao X, Zheng S (2009) Development of polymer-based nanosized hydrated ferric oxides (HFOs) for enhanced phosphate removal from waste effluents. Water Res 43:4421–4429

Peng L, Dai H, Wu Y, Peng Y, Lu X (2018) A comprehensive review of phosphorus recovery from wastewater by crystallization processes. Chemosphere 197:768–781

Rostamian R, Najafi M, Rafati AA (2011) Synthesis and characterization of thiol-functionalized silica nano hollow sphere as a novel adsorbent for removal of poisonous heavy metal ions from water: kinetics, isotherms and error analysis. Chem Eng J 171:1004–1011

Shi W, Fu Y, Jiang W, Ye Y, Kang J, Liu D, Ren Y, Li D, Luo C, Xu Z (2019) Enhanced phosphate removal by zeolite loaded with Mg–Al–La ternary (hydr) oxides from aqueous solutions: performance and mechanism. Chem Eng J 357:33–44

Su Y, Yang W, Sun W, Li Q, Shang JK (2015) Synthesis of mesoporous cerium–zirconium binary oxide nanoadsorbents by a solvothermal process and their effective adsorption of phosphate from water. Chem Eng J 268:270–279

Sunding MF, Hadidi K, Diplas S, Løvvik OM, Norby TE, Gunnæs AE (2011) XPS characterisation of in situ treated lanthanum oxide and hydroxide using tailored charge referencing and peak fitting procedures. J Electron Spectrosc Relat Phenom 184:399–409

Suresh Kumar P, Ejerssa WW, Wegener CC, Korving L, Dugulan AI, Temmink H, van Loosdrecht MCM, Witkamp G (2018) Understanding and improving the reusability of phosphate adsorbents for wastewater effluent polishing. Water Res 145:365–374

Tran HN, You S, Hosseini-Bandegharaei A, Chao H (2017) Mistakes and inconsistencies regarding adsorption of contaminants from aqueous solutions: a critical review. Water Res 120:88–116

Vikrant K, Kim K, Ok YS, Tsang DC, Tsang YF, Giri BS, Singh RS (2018) Engineered/designer biochar for the removal of phosphate in water and wastewater. Sci Total Environ 616:1242–1260

Wan J, Zhu C, Hu J, Zhang TC, Richter-Egger D, Feng X, Zhou A, Tao T (2017) Zirconium-Loaded Magnetic Interpenetrating Network Chitosan/Poly (vinyl alcohol) Hydrogels for Phosphorus Recovery from the Aquatic Environment. Appl Surf Sci 423:484–491

Wang Z, Guo H, Shen F, Yang G, Zhang Y, Zeng Y, Wang L, Xiao H, Deng S (2015) Biochar produced from oak sawdust by Lanthanum (La)-involved pyrolysis for adsorption of ammonium ($NH_4^+$), nitrate ($NO_3^-$), and phosphate ($PO_4^{3-}$). Chemosphere 119:646–653

Wu B, Fang L, Fortner JD, Guan X, Lo IMC (2017) Highly efficient and selective phosphate removal from wastewater by magnetically recoverable $La(OH)_3/Fe_3O_4$ nanocomposites. Water Res 126:179–188

Xie J, Wang Z, Lu S, Wu D, Zhang Z, Kong H (2014) Removal and recovery of phosphate from water by lanthanum hydroxide materials. Chem Eng J 254:163–170

Zhang J, Shen Z, Shan W, Mei Z, Wang W (2011) Adsorption behavior of phosphate on lanthanum(III)-coordinated diamino-functionalized 3D hybrid mesoporous silicates material. J Hazard Mater 186:76–83

Zhang L, Zhou Q, Liu J, Chang N, Wan L, Chen J (2012) Phosphate adsorption on lanthanum hydroxide-doped activated carbon fiber. Chem Eng J 185-186:160–167

Zhou H, Li X, Xu G, Yu H (2018) Overview of strategies for enhanced treatment of municipal/domestic wastewater at low temperature. Sci Total Environ 643:225–237